ELSEVIER

Journal of Fluids and Structures 25 (2009) 284–303

JOURNAL OF FLUIDS AND STRUCTURES

www.elsevier.com/locate/jfs

Theoretical analysis of hydrostatic implodable volumes with solid inner structures

J.J. Cor*, T.F. Miller

Applied Research Laboratory, The Pennsylvania State University, P.O. Box 30, State College, PA 16804, USA

Received 18 January 2007; accepted 10 April 2008
Available online 7 July 2008

Abstract

The basic analytical theory for hydrostatically caused implosions of spherical volumes, which has been known for nearly a century, has been extended for the treatment of annular volumes with solid inner structures. Theoretical analyses are developed that treat the inner structure as infinitely hard, elastically deformable, plastically deformable or shattering under the influence of the pressure from the surrounding implosion event. Parametric studies are made of the effect that the inner structure's geometric and material properties have on the pressure field of the surrounding water. It is concluded that the pressure waves produced by the imploding volume are significantly affected by the existence of an inner structure and the inner structure's physical properties. This is an important consideration in assessing the effect of an underwater implosion event on nearby structures.

Keywords: Potential flow; Underwater implosion

1. Introduction

Lord Rayleigh (1917), and subsequently Lamb (1932), defined the basic equations of bubble collapsing theory. This theory was subsequently modified by other workers to incorporate the internal gas pressure that permitted the analysis of the oscillating bubble phenomenon. In this theory, the bubble initially contracts under the outside pressure of the liquid. At some point, the interior gas pressure is increased to the point where it balances the combined hydrostatic and hydrodynamic heads, and the gas volume stops decreasing. Then the higher relative interior pressure acts to force the gas bubble radius outward until the exterior hydrostatic pressure is enough to counter the interior gas pressure plus the gas hydrodynamic head. The bubble motion reverses itself once again, and the bubble begins to contract. This cycle will continue until losses act to stop it. The gas volume oscillations also produce oscillations in the pressure field of the surrounding seawater. The oscillating pressure field can serve as an acoustic source, or if sufficiently large, can produce a pressure wave with sufficient energy to damage nearby structures.

An implodable volume can be defined as any pressure housing, containing a non-compensated compressible volume of gas at a pressure below the external sea pressure, which has the potential to collapse. There is concern that under the wrong circumstances, the pressure pulses produced by the collapsing volume can damage nearby submersibles or other objects. This was dramatically demonstrated in 2001 at the Kamioka Observatory, in its Super-Kamiokande experiment

*Corresponding author. Tel.: +1 814 865 6469; fax: +1 814 863 7842.
E-mail address: jjc19@psu.edu (J.J. Cor).

0889-9746/$ - see front matter © 2008 Elsevier Ltd. All rights reserved.
doi:10.1016/j.jfluidstructs.2008.04.003

Nomenclature

A	surface area (m^3)
C	speed of sound (m/s) or circumference (m)
E	bulk modulus of elasticity (Pa)
F	required function
K_L	bulk modulus of elasticity (Pa)
p	pressure (Pa)
P	gas (acoustic) pressure (Pa)
q	kinetic energy (m^2/s^2)
r	radius (m)
R	implodable volume outer radius (m)
t	time (s), thickness (m)
U	velocity (m/s)
v	solid velocity (m/s)
V	volume (m^3)
γ	ratio of specific heats
δ	differential distance (m)
ε	strain
μ	dynamic viscosity ($N\,s/m^2$)
ρ	density (kg/m^3)
σ	stress (Pa)
ϕ	stream function

Subscripts

a	acoustic
EQ	equilibrium
g	gas
H	hoop
L	liquid or longitudinal
m	metal
O	reference condition
r	radial
V	value at shell inner surface
∞	far field (infinity)
θ	azimuthal

dedicated to neutrino research.[1] Over 5000 of this facility's photomultiplier tubes were destroyed in a cascading underwater implosion initiated by the collapse of a single tube. The importance of the failure of implodable volumes is also mentioned in the US Navy Unmanned Undersea Vehicle Master Plan (2004):

> Ship deployed [Unmanned Undersea Vehicle] UUV systems must meet very stringent requirements to be authorized for submarine installation, including, but not limited to, shock requirements, battery (or other energy source) certification, and implodable volume requirements … Obtaining these certifications can result in significant costs and delays in deploying these systems. Investments should be made early to determine how UUV systems could be designed and built to cost effectively meet ship certification requirements. [Underlined emphasis is ours.]

However, the analysis procedure associated with defining and evaluating implodable volumes is very conservative (Joint Fleet Maintenance Manual, 2006):

> [An implodable volume is] any pressure housing containing a non-compensated compressible volume at a pressure below the external sea pressure (at any depth down to the maximum operating depth) which has the potential to collapse. The outer shell volume is used when calculating the volume of an implodable. Subtracting the volume of items internal to the implodable is not allowed. Externally mounted lights, gauges, bottles/flasks, spheres/tanks and beacons are examples of implodable items. [Again, the underlined emphasis is ours.]

Using the above criteria, the energy available from an implodable volume can be approximated by the P–dV work required to compress the volume such that the interior volume pressure is equal to the hydrostatic pressure. This approach leads to such misleading statements in the popular press as: "… The implosion of even a fist-sized volume of air at Titanic depth would be the equivalent of five sticks of dynamite going off …"[2] Of course, the rate at which the energy is released does as much to define the explosive effect as the total energy released. Another important consideration is the presence of non-imploding or energy-absorbing compressible volumes within the outer shell volume. Safety is clearly a vital consideration when dealing with nearby implodable volumes; however, we feel that greater physical understanding of the implosion process benefits not only safety, but economic and system performance considerations as well.

Fluid–structure interactions have been studied previously in related applications. The interaction of an external explosion with a deformable or collapsible inner structure was investigated by Iakovlev (2004, 2006). The interaction of a bubble caused by an underwater explosion with an object on the water surface was studied by Zong (2004) and Klaseboer et al. (2005). Kalumuck et al. (1995) studied bubble interaction with nearby bodies using three-dimensional

[1] Details of this event were obtained from Fermi News, vol. 24, no. 19, 23 November 2001.

[2] Quote comes from the article "Contents Under Pressure," Paula Parisi, Wired Magazine, Issue 6.02, February 1998.

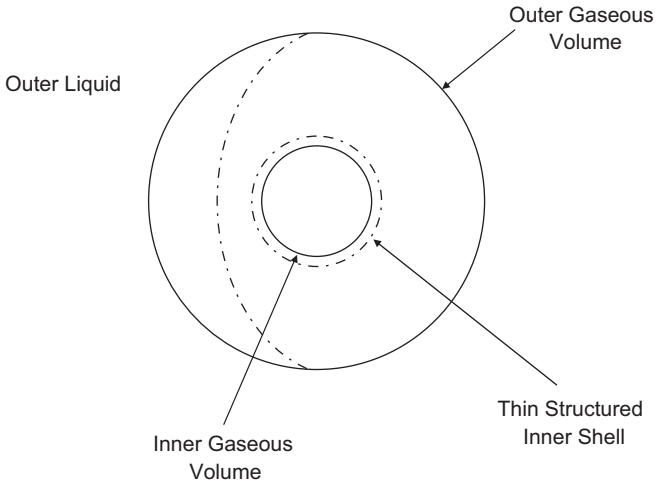

Fig. 1. Implodable volumes for spherical geometry.

boundary-element based computer codes. While the analysis of real world geometries in studies such as these requires substantial computational resources, the objective of the present work is more modest: evaluating the effect of internal structure on the behavior of spherical implodable volumes, with the goal of eventually assessing the degree of conservatism of the criteria described above.

In addition to being the unintended source of the spectacular Super-Kamiokande failure discussed above, glass volumes (in this case spheres) have also been safely employed as acoustic sources for studies of implodable volumes (Arons et al., 1948; Ghiotto and Penrose, 2000). They are suspended on a cable and at a desired depth are struck by a weight causing an instantaneous fracturing of the sphere. Implodable volumes are of greater concern to operators of deep-diving submersibles because the pressure pulse produced may have the potential to damage or sink the vehicle. Because of the practicality of the analysis of spheres (as models for bubbles and acoustic generators), little interest has been directed at geometries containing interior non-imploding (or delayed imploding) volumes. However, annular volumes, or volumes containing non-implodable centers may be of more practical interest as more closely mimicking implodable volumes that might be formed external to submerged vessels. And while no cylindrical analog exists for the Rayleigh collapse model presented below, the Rayleigh model has been found to closely approximate the behavior of large aspect ratio cylindrical geometries, when the proper scaling is applied (Goodwin et al., 1999). Therefore, this paper explores spherical geometries with inner shells that are infinitely strong, brittle, plastic, or elastic, and house an additional implodable volume; see Fig. 1.

2. Basic theory—spherical volume with infinitely strong inner structure

Starting with the assumption of an irrotational and incompressible external fluid, its movement can be described with the Bernoulli equation:

$$\frac{\partial\phi}{\partial t} - q + F(t) = \frac{p}{\rho}, \tag{1}$$

where ϕ is the velocity potential, q is the kinetic energy, p is the liquid pressure, ρ is the liquid density and $F(t)$ is a function of time. The velocity potential must satisfy Poisson's equation in spherical coordinates:

$$\frac{\partial}{\partial r}\left(r^2\frac{\partial\phi}{\partial r}\right) = 0. \tag{2}$$

A solution to Eq. (2) is

$$\phi = \left(\frac{R^2}{r}\right)\left(\frac{\mathrm{d}R}{\mathrm{d}t}\right), \tag{3}$$

where R is the radius of the gaseous space. The velocity of the fluid then is

$$U = -\frac{\partial \phi}{\partial r} = \left(\frac{R^2}{r^2}\right)\left(\frac{dR}{dt}\right). \tag{4}$$

Substituting the values for ϕ and U into Eq. (1) yields:

$$\frac{1}{r}\left[R^2\left(\frac{d^2R}{dt^2}\right) + 2R\left(\frac{dR}{dt}\right)^2 - \frac{1}{2}\left(\frac{R^4}{r^4}\right)\left(\frac{dR}{dt}\right)^2\right] + F(t) = \frac{p}{\rho}. \tag{5}$$

Far away from the sphere the pressure is p_∞, which defines $F(t)$. This substitution gives the final form for the hydrodynamic equation of fluid motion:

$$\frac{1}{r}\left[R^2\left(\frac{d^2R}{dt^2}\right) + 2R\left(\frac{dR}{dt}\right)^2 - \frac{1}{2}\left(\frac{R^4}{r^4}\right)\left(\frac{dR}{dt}\right)^2\right] = \frac{p - p_\infty}{\rho}. \tag{6}$$

At the surface of the gas volume ($r = R$, $p = p_g$), this becomes:

$$R\left(\frac{d^2R}{dt^2}\right) + \frac{3}{2}\left(\frac{dR}{dt}\right)^2 = \frac{p_g - p_\infty}{\rho}. \tag{7}$$

For an isentropic expansion/contraction of the ideal gas:

$$\frac{p_g}{p_{g_o}} = \left(\frac{V_O}{V}\right)^\gamma, \tag{8}$$

where γ is the ratio of specific heats and the subscript O refers to initial conditions. If the gas volume surrounds an inner concentric spherical shell of radius R_V:

$$\frac{p_g}{p_{g_o}} = \left[\frac{R_O^3 - R_V^3}{R^3 - R_V^3}\right]^\gamma. \tag{9}$$

The final equation of motion for the volume is then

$$R\left(\frac{d^2R}{dt^2}\right) + \frac{3}{2}\left(\frac{dR}{dt}\right)^2 = \frac{1}{\rho}\left\{p_{g_o}\left[\frac{R_O^3 - R_V^3}{R^3 - R_V^3}\right]^\gamma - P_\infty\right\}. \tag{10}$$

Eq. (10) is readily solvable using the Runge–Kutta–Nystrom method with a time step on the order of 10^{-7} s.

Vokurka (1985) showed that the pressure in the liquid surrounding the implodable volume is given by

$$p_a = \frac{R}{r}P_a + \frac{1}{2}\frac{R}{r}\left(\frac{dR}{dt}\right)^2 - \frac{1}{2}\left(\frac{R}{r}\right)^4\left(\frac{dR}{dt}\right)^2, \tag{11}$$

where p_a refers to the local acoustic (local minus hydrostatic) pressure in the liquid and P_a refers to the acoustic pressure of the gas.

A comparison was made of the predictions using the above-idealized analysis with the measurements of Buogo and Cannelli (2002), who generated a bubble from an underwater spark located 2.5 m below the surface of a water tank. The variation of the bubble's radius with time is shown in Fig. 2. Also shown in this figure is the radius predicted for the first expansion–compression cycle by integrating Eq. (10). The analysis was made using the reported value for the pressure at the peak radius of 35 mm (0.3 bars) as the initial pressure of the collapsing volume, and by setting R_V in Eq. (10) to zero. The radius of the bubble decreases to lower levels in the measurements due to thermal losses and due to the fact that the experimental bubble was initiated from an energy release, effectively starting from a zero radius, the analysis of which is beyond the scope of the current analysis. Overall, agreement is close between the experiment and modeling for the majority of the first bubble cycle.

The first cycle, being the one most important in assessing the damage done to surrounding underwater structures by a collapsing volume, is the cycle of primary interest in this work. Subsequent attenuation and oscillations in the collapsing bubble structure, notable fields of enquiry in and of themselves, have secondary importance in considering the damage

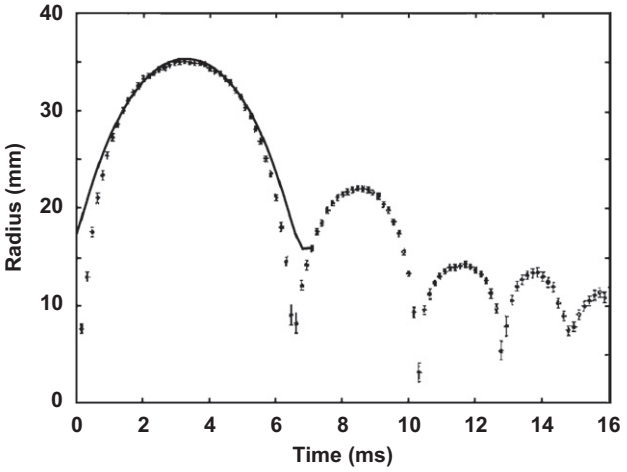

Fig. 2. Comparison of gas bubble radius versus time measurements of Buogo and Cannelli (2002) (symbols) with predictions using the current analysis (solid line).

Table 1
Sample analysis problem conditions

Initial sphere radius	50 cm
Strong inner shell radius	5 cm
Initial sphere pressure	1 atm
Time increment of calculations	10^{-7} s
Sphere depth	100 m
Liquid medium	Water
Gas medium	Air

caused by collapsing underwater volumes. Thus, the irrotational, isentropic analysis described in this paper can be considered a useful tool over the time scales where the greatest damage can be inflicted on surrounding structures.

An example analysis was made of an implodable spherical volume under the conditions given in Table 1. Fig. 3 shows the calculated radius for the volume through the first cycle of oscillation. The volume reaches its minimum and returns to its initial value in approximately 31 ms, after which the cycle repeats itself. Also shown in Fig. 3 are results where the volume depth is at half and twice the baseline depth of 100 m. The effect of increasing depth is to decrease both the period of oscillation and the minimum radius the gas volume. Fig. 4 shows the velocity of the volume's outer surface for the baseline depth and half and twice the baseline depth. The peak volume surface velocities increase with depth. Fig. 5 shows how the interior gas pressure varies with time. Also shown are pressures when the initial and shell radii are at half and twice the baseline value. The peak pressure does not vary appreciably with the radii, but the period of oscillation increases with the value of the radii. Figs. 3–5 show that the minimum radius, peak velocity and peak pressure all occur at the same point. Fig. 6 presents a sequence of values of the liquid acoustic pressure, up to the peak pressure, calculated using Eq. (11). Out to a range of 300 cm from the volume's center (or approximately 250 cm from the baseline bubble radius), the acoustic pressure excursions are still at 10 atm.

3. Inner shell deformation or failure

3.1. Stress analysis

For all the analyses in Section 2, the inner shell was considered indestructible and non-deformable. Cases now are analyzed where these assumptions are removed, and the inner shell is considered to fracture in a brittle fashion, or deform plastically or elastically. The analyses below are made with the assumption that the inner, solid structure responds instantaneously to disturbances. This assumption is considered reasonable for the characteristic times of

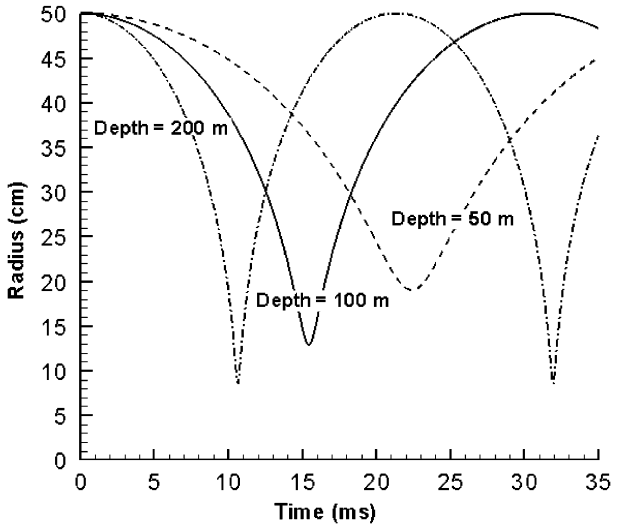

Fig. 3. Spherical volume radius under conditions given in Table 1. Dashed lines present results for depth variations from the baseline value of 100 m.

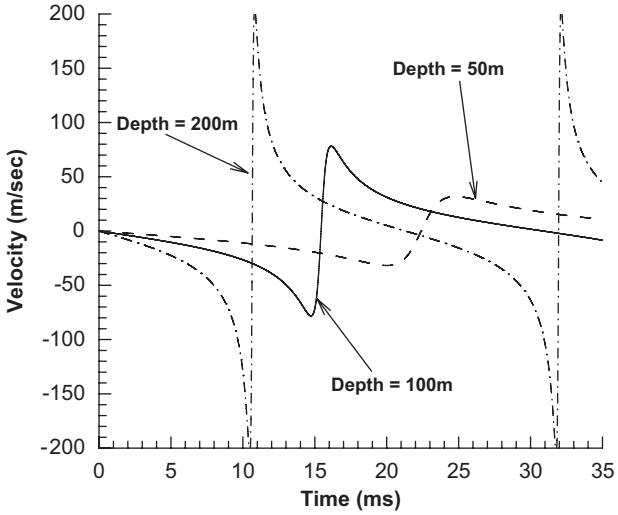

Fig. 4. Spherical volume surface velocity under conditions given in Table 1. Dashed lines present results for depth variations from the baseline value of 100 m.

this problem. An iron shell, for instance, has a sonic velocity of 4500 m/s, comparable to the sonic velocity in water. An iron shell of 10 mm thickness, for example, would have a characteristic response time on the order of 10^{-6} s, which is two-to-three orders or magnitude lower than the typical periods associated with the implodable volume oscillations analyzed below.

For all cases, the thin-walled assumption is made for computing inner shell stresses. For shells with thickness less than one-tenth, the inner wall radius, this assumption results in errors of less than 5% of the actual wall stress. For a thin-walled spherical vessel, the normal stress in the wall is given by

$$\sigma = \frac{1}{2}(p_{\text{inner}} - p_{\text{outer}})\frac{r}{t}, \tag{12}$$

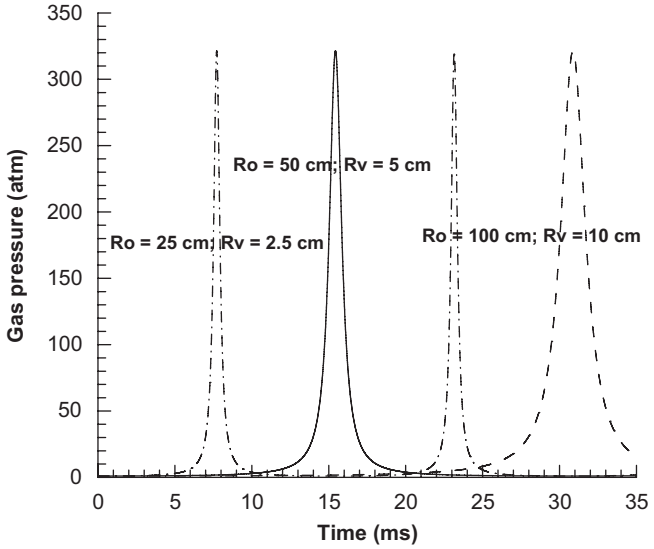

Fig. 5. Spherical volume gas pressure under conditions given in Table 1. Dashed lines present results for radius variations from the baseline values of initial gas radius (R_O) of 50 cm and inner shell radius (R_V) of 5 cm.

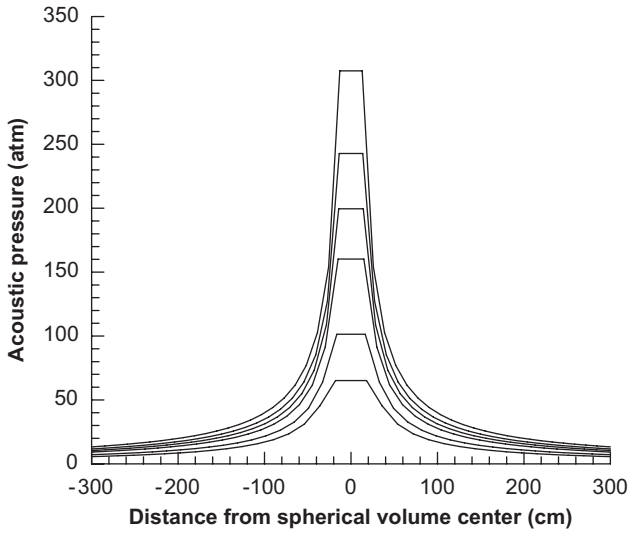

Fig. 6. Acoustic pressure in liquid surrounding spherical volume under conditions given in Table 1. In order of increasing magnitude, the data are presented at 14.6, 14.8, 15, 15.1, 15.2, and 15.5 ms (peak magnitude of acoustic field).

where t is the thickness of the vessel wall and the outer pressure is that of the imploding volume surrounding the inner shell. The wall stresses are principal stresses and it was assumed that failure occurs in one of the shell's principal planes.

3.2. Brittle shell

For the case of a brittle shell, when the principal stress exceeds the maximum allowable stress, the shell was assumed to shatter. Such an assumption might be appropriate for a cast iron or composite material, for instance. When the shell shatters, the gaseous volume's outer radius is the radius of the gas volume at the point of failure, R, and it was assumed

Table 2
Sample brittle inner shell problem conditions

Initial gas volume radius	50 cm
Brittle shell outer radius	40 cm
Brittle shell thickness	5 mm
Initial gas pressure	1 atm
Time increment of calculations	10^{-7} s
Gas volume depth	100 m
Liquid medium	Water
Gas medium	Air
Shell failure stress	0.33 GPa

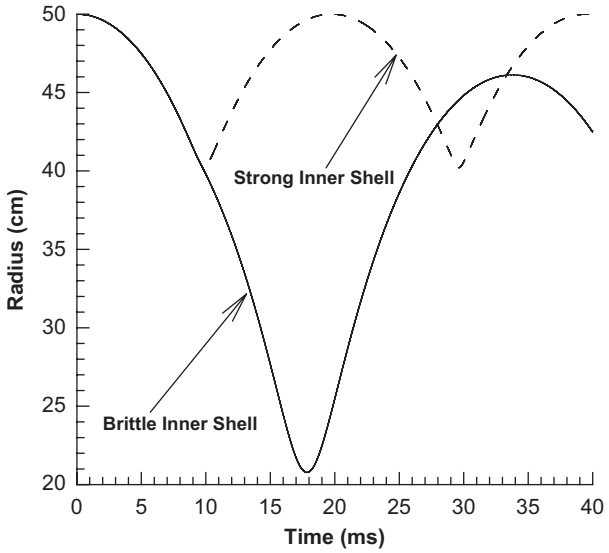

Fig. 7. Spherical volume radius under conditions given in Table 2, assuming a strong inner shell (dashed line) and a brittle inner shell (solid line).

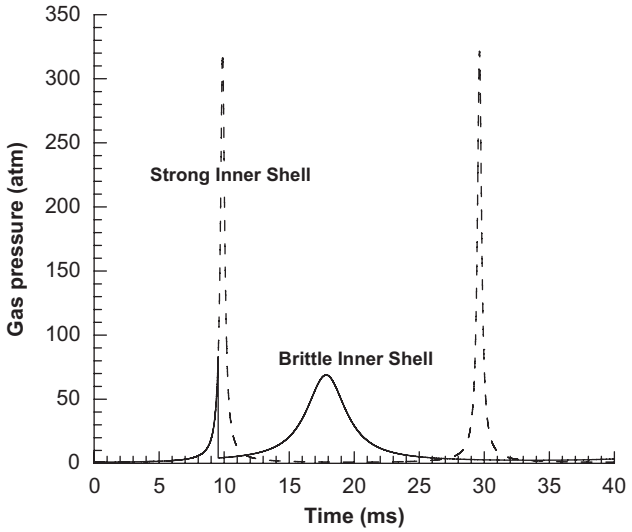

Fig. 8. Spherical volume gas pressure under conditions given in Table 2, assuming a strong inner shell (dashed line) and a brittle inner shell (solid line).

that the inner radius became zero. It was assumed that the gas that was in the inner shell, at p_{inner}, and the surrounding volume, at p_{gas}, mix insentropically, resulting in a new pressure of:

$$p_{\text{new}} = p_{\text{inner}}\left(\frac{R_V}{R}\right)^3 + p_{\text{gas}}\left[1 - \left(\frac{R_V}{R}\right)^3\right]; \tag{13}$$

R_V in Eq. (13) is the inner radius of the shell before failure.

The isentropic mixing assumption is one limiting case of conditions inside the gas volume at the point of shell failure. Another limit on the conditions would be to assume that the pressure is discontinuous between p_{inner} and p_{gas} at the point of shell failure, creating an imploding shock wave. A detailed analysis of this phenomenon, including its reflection at the volume center and its interaction with the surrounding liquid, was deemed beyond the current scope of this effort but is an important venue for future research.

An example problem with a brittle shell was run using the conditions shown in Table 2. The failure stress was chosen to be that consistent with cast iron. The volume geometry chosen was spherical and was analyzed using the potential flow solution described in Section 2. It can be seen that the initial gas radius and shell radius are much closer in value than they were in Table 1. This is because volume varies with the radius cubed, and the effect of shell failure (or deformation) only becomes significant when the inner shell volume becomes large relative to the initial gas volume.

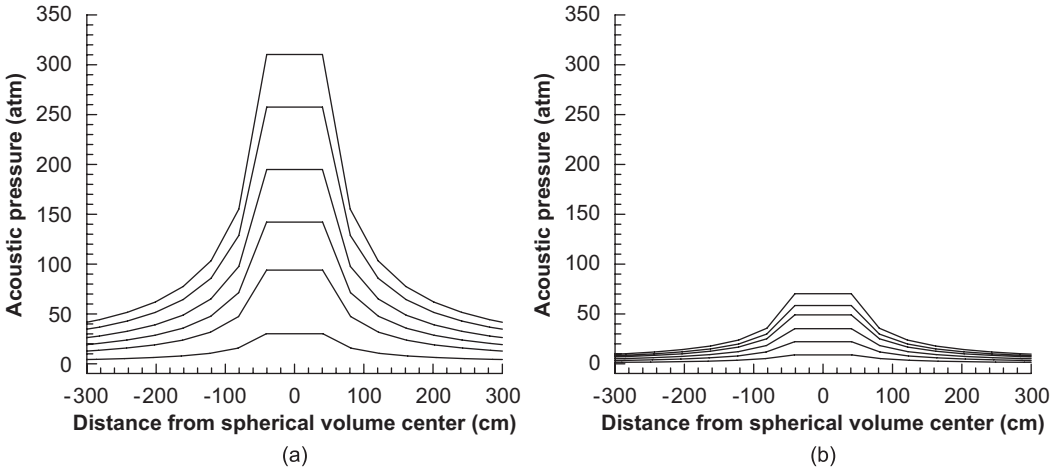

Fig. 9. Acoustic pressure in liquid surrounding spherical volume under conditions given in Table 2, assuming a strong inner shell (a) and brittle inner shell (b). In order of increasing magnitude, the data for (a) are presented at 9.33, 9.59, 9.67, 9.73, 9.79, and 9.87 ms (the time of peak magnitude of the acoustic field). In order of increasing magnitude, the data for (b) are presented at 9.01, 9.25, 9.37, 9.45, 9.49, and 9.53 ms (the time of peak magnitude of the acoustic field).

Table 3
Sample plastic inner shell problem conditions

Initial gas volume radius	100 cm
Brittle shell outer radius	88 cm
Brittle shell thickness	8 mm
Initial gas pressure	1 atm
Initial inner shell pressure	1 atm
Time increment of calculations	10^{-7} s
Gas volume depth	300 m
Liquid medium	Water
Gas medium	Air
Material viscosity	3000 N s/m^2
Plasticity modulus	0.53 GPa
Modulus of elasticity[a]	8 GPa

[a]Used for elastic shell analysis.

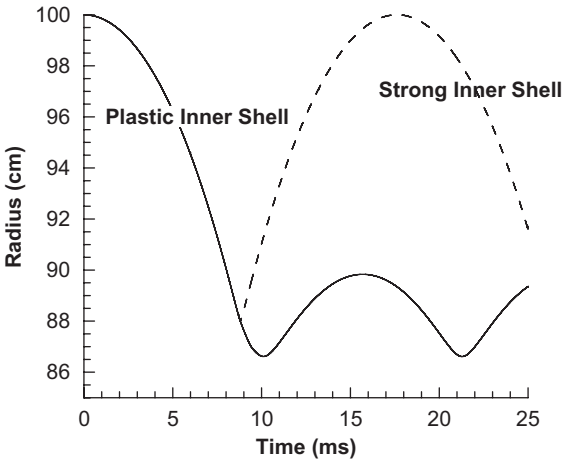

Fig. 10. Spherical volume radius under conditions given in Table 3, assuming a strong inner shell (dashed line) and a plastic inner shell (solid line).

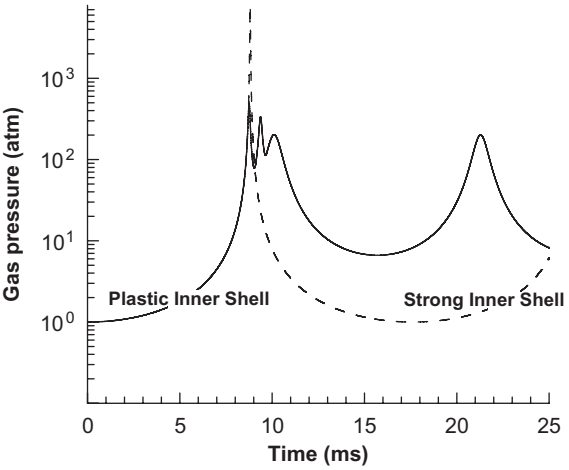

Fig. 11. Spherical volume radius under conditions given in Table 3, assuming a strong inner shell (dashed line) and a plastic inner shell (solid line).

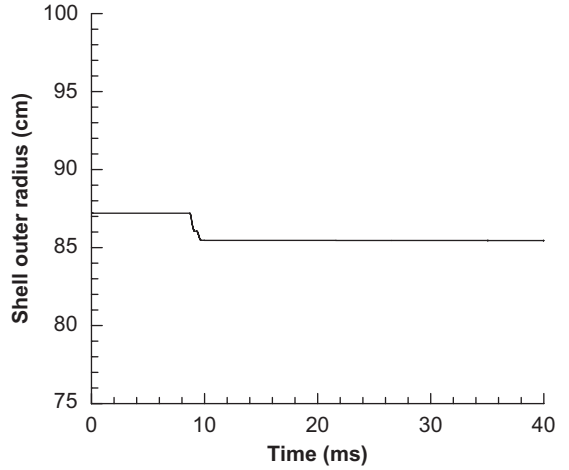

Fig. 12. Inner shell's outer radius under conditions given in Table 3, assuming that the inner shell deforms plastically.

The analysis was first run assuming an infinitely strong inner shell that was not allowed to fail, and then was run assuming the shell is brittle. With the brittle shell, failure occurred at 9.5 ms at a gas pressure of 83 atm. Fig. 7 shows the calculated radius for each of these cases. The failure of the shell reduces the minimum gas volume radius and increases the period of oscillation. Fig. 8 shows a plot of the gas pressure assuming a strong and brittle inner shell. The effect of shell failure is to reduce the peak gas pressure by over a factor of four.

The effect on the liquid pressure field that a failure of the inner shell would cause is of great concern for nearby submersibles. A comparison of the liquid pressure field with the strong shell and brittle shell (Fig. 9) shows that the failure of the shell significantly reduces the acoustic pressure in the water. The times in Fig. 9(b) are centered on the point of shell failure, which can be identified by the first brittle shell peak in Fig. 8. At a distance of 300 cm the peak acoustic pressure in the water is reduced by a factor of four when the shell fails by brittle fracture.

3.3. Plastic shell

A model for the plastic deformation of casings under external loads was developed by Tan et al. (2003). Tan et al. used the following constitutive law for viscoplastic (ignoring elastic) deformation:

$$\sigma_\theta - \sigma_r = \mathrm{sgn}\left(\frac{\mathrm{d}r_2}{\mathrm{d}t}\right)2K - 4\mu\left(\frac{\mathrm{d}v}{\mathrm{d}r}\right), \tag{14}$$

where σ_θ is the azimuthal stress, σ_r is the radial stress, $\mathrm{d}r_2/\mathrm{d}t$ is the velocity on the outer surface of the casing, μ is the dynamic viscosity, v is the radial velocity in the casing and sgn is the sign function. Tan et al. also expressed the conservation of mass and Euler's equation as:

$$\frac{\mathrm{d}v}{\mathrm{d}r} + N\frac{v}{r} = 0, \tag{15}$$

and

$$\rho_m\left(\frac{\mathrm{d}v}{\mathrm{d}t} + v\frac{\mathrm{d}v}{\mathrm{d}r}\right) = \frac{\mathrm{d}\sigma_r}{\mathrm{d}r} + \frac{N}{r}(\sigma_r - \sigma_\theta), \tag{16}$$

where $N = 1$ for cylindrical geometries and $N = 2$ for spherical geometries, and ρ_m is the density in the casing.

Combining Eqs. (14)–(16), it can be shown that the equation of motion in for the spherical casing is

$$\rho_m r_1\left(1 - \frac{r_1}{r_2}\right)\ddot{r}_1 + \rho_m\left\{2\left(1 - \frac{r_1}{r_2}\right) - \frac{1}{2}\left[1 - \left(\frac{r_1}{r_2}\right)^4\right]\right\}(\dot{r}_1)^2 = \sigma_r(r_2) - \sigma_r(r_1) - \mathrm{sgn}(\dot{r}_2)4K\ln\left(\frac{r_2}{r_1}\right) - \frac{16}{3}\mu\left[1 - \left(\frac{r_1}{r_2}\right)^2\right]\frac{\dot{r}_1}{r_1}, \tag{17}$$

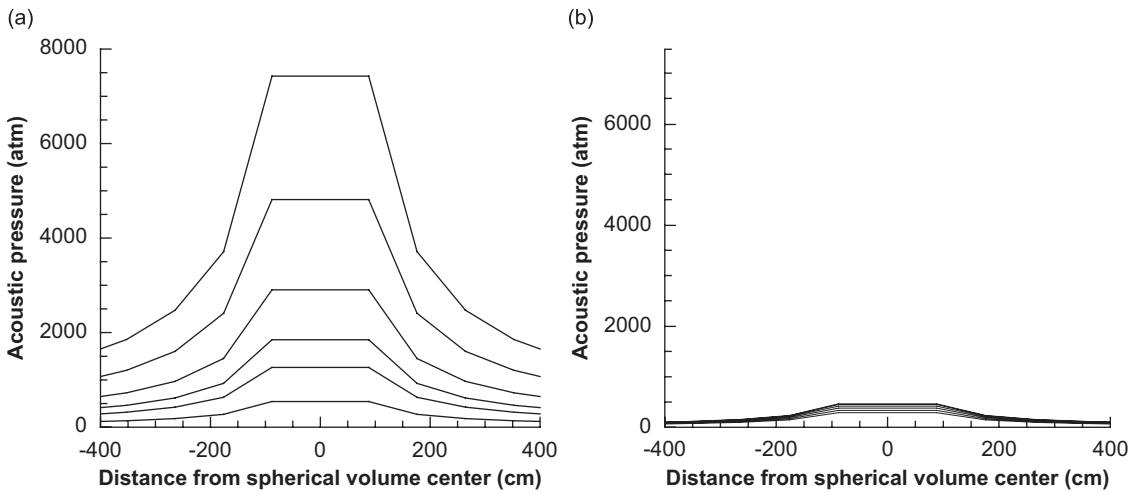

Fig. 13. Acoustic pressure in liquid surrounding spherical volume under conditions given in Table 3, assuming that the inner shell does not fail or deform (a) and assuming that the inner shell deforms plastically (b). In order of increasing magnitude, the data in (a) are presented at 8.73, 8.76, 8.77, 8.78, 8.79, and 8.81 ms (the time of peak magnitude of the acoustic field). In order of increasing magnitude, the data in (b) are presented at 8.70, 8.71, 8.72, 8.73, 8.74, and 8.75 ms (the time of peak magnitude of the acoustic field).

where r_2 is the outer casing radius and r_1 is the inner casing radius. For the current application, $\sigma_r(r_2)$ is the negative of the gas pressure of the implodable volume and $\sigma_r(r_1)$ is the negative of the gas pressure inside the shell, which now varies as the shell expands or contracts. The overdots refer to the first or second derivative with respect to time. It was assumed that the inner shell's initial pressure was the same as the initial pressure of the implodable volume and that it obeyed the ideal gas law as the inner shell's volume changed. As the implodable volume expanded or contracted, Eq. (17) was integrated, using the Runge–Kutta–Nystrom method, to obtain the inner radius of the plastic shell as a function of time. Assuming the shell material was incompressible, mass conservation was used to calculate the outer shell radius from the updated value of the inner shell radius.

An example problem was run using the conditions listed in Table 3. Shell material properties were taken from those reported by Tan et al. To isolate the effect of plastic deformation, the shell was not allowed to fail, although stresses would be great enough to have done so. Fig. 10 shows the trace of the gaseous volume's radius versus time when the inner shell is infinitely strong, and when it is plastic. Fig. 11 shows the corresponding gas pressures for the infinitely strong and plastic shells. The scale in Fig. 11 has been changed to logarithmic, to better display the pressure traces on the same graph. It can be seen that the plastic deformation of the shell has a dramatic effect on reducing the maximum gas pressure inside the implodable volume. Fig. 12 shows the variation of the plastic shell's outer radius with time. After the outer gas pressure reaches a critical level, the shell plastically deforms to a new radius. This newly deformed shell

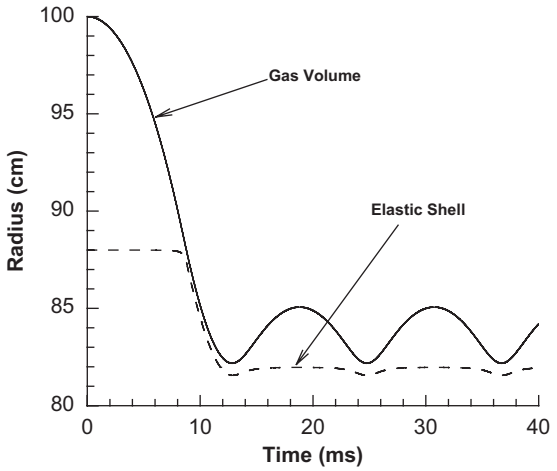

Fig. 14. Spherical gas volume radius (solid line) and shell outer radius (dashed line) under conditions given in Table 3, assuming that the inner shell deforms elastically.

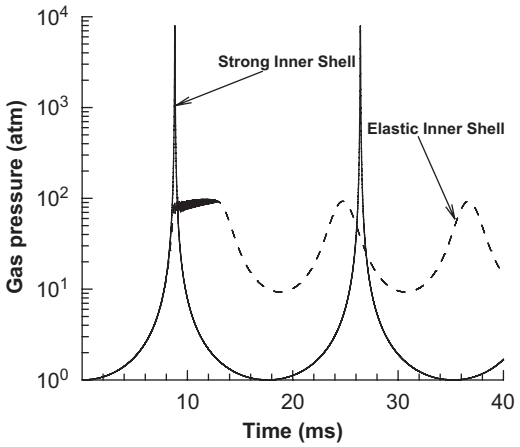

Fig. 15. Spherical volume gas pressure under conditions given in Table 3, assuming a strong inner shell (solid line) and an elastic inner shell (dashed line).

only decreases in volume slightly under further loading from the outer pressure. This adjustment in radius creates the dramatic decrease in gas pressure observed in Fig. 11. It is noted in Fig. 12 that the shell has a brief period of zero slope during its deflection to the smaller radius, and the time of this zero deflection accounts for the double spike in the gas pressure seen in Fig. 11 before it adjusts to its new, lower level.

A comparison of the liquid acoustic pressure fields assuming a strong and plastic shell is presented in Fig. 13. The results show that the plastic deformation of the shell reduces farfield pressure excursions by two orders of magnitude.

3.4. Elastic shell

For a purely elastic thin shell, the average azimuthal strain is

$$\varepsilon = \frac{\sigma_\theta}{E}, \tag{18}$$

where E is the bulk modulus of elasticity. The differential change of circumference (δC) is found from

$$\delta C = C\varepsilon = \frac{2\pi\sigma_\theta}{E}. \tag{19}$$

The change in radius is then

$$\delta r = \frac{\delta C}{2\pi} = \frac{r\sigma_\theta}{E}. \tag{20}$$

In terms of the inner shell radius (r_1), the inner shell strain is

$$\varepsilon_1 = \frac{\delta r_1}{r_1} = \frac{\sigma_\theta}{E}. \tag{21}$$

If the shell material is incompressible, the outer shell radius (r_2) must then be (neglecting higher order terms):

$$\varepsilon_2 = \varepsilon_1 \left(\frac{r_1}{r_2}\right)^3. \tag{22}$$

Updated inner and outer radii are then given by

$$r_1(\text{new}) = r_1(1+\varepsilon_1), \quad r_2(\text{new}) = r_2(1+\varepsilon_2)\cdot \tag{23}$$

An example analysis for an elastic shell was run under the conditions given in Table 3. The modulus of elasticity chosen was that for iron. The shell was not allowed to fail so that the effect of the elastic deformation could be isolated. Fig. 14 shows the variation of the gaseous volume's radius and the shell's outer radius with time. The gaseous radius behaves in a manner similar to that found for the plastic shell (Fig. 10), although in Fig. 14 it assumes a smaller

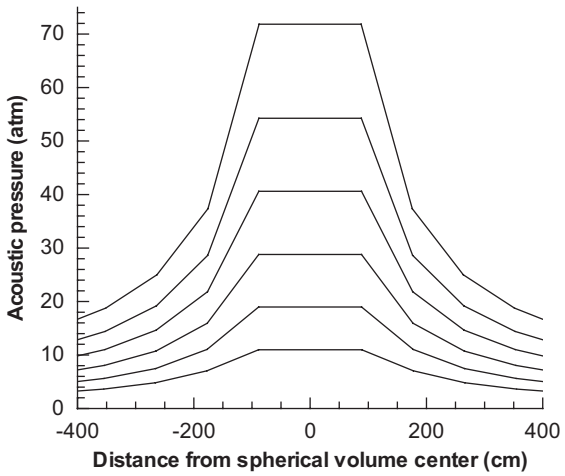

Fig. 16. Acoustic pressure in liquid surrounding spherical volume under conditions given in Table 3, assuming that the inner shell deforms elastically. In order of increasing magnitude, the data are presented at 8.50, 8.56, 8.62, 8.68, 8.74, and 8.85 ms (the time of peak magnitude of the acoustic field).

minimum radius in its oscillations. This is because the shell radius reaches a smaller minimum value than it did in the plastic case (Fig. 12). The elastic shell, it is also noted, oscillates about a new, lower value after an initial contraction. Fig. 15 shows the variation of the gas pressure with time assuming an elastic inner shell, with the pressure trace for the strong inner shell included for reference. The new equilibrium behavior in this figure is similar to that shown in Fig. 11 for the plastic inner shell, although there is a high-frequency oscillation present in Fig. 15 during the first contraction of the elastic shell.

The results of the analysis of deformable shells indicate there is some non-recoverable work that is done in compressing the shell to a new equilibrium value. This is true whether the shell is deforms elastically or plastically. The isentropic assumption for the gas may have to be modified to more closely represent the acoustic behavior of the imploding volume for these cases.

Fig. 16 shows the calculated liquid acoustic pressure for the case of an elastic inner shell. The scale of this figure was expanded relative to Fig. 13, so that the pressure excursions could be displayed in detail. The acoustic excursions are significantly reduced over those found assuming an infinitely strong inner shell (Fig. 13(a)) and the plastic inner shell (Fig. 13(b)). This is not surprising when the peak gas pressure for the elastic shell (Fig. 15) is compared to the peak pressure shown for the plastic shell (Fig. 11).

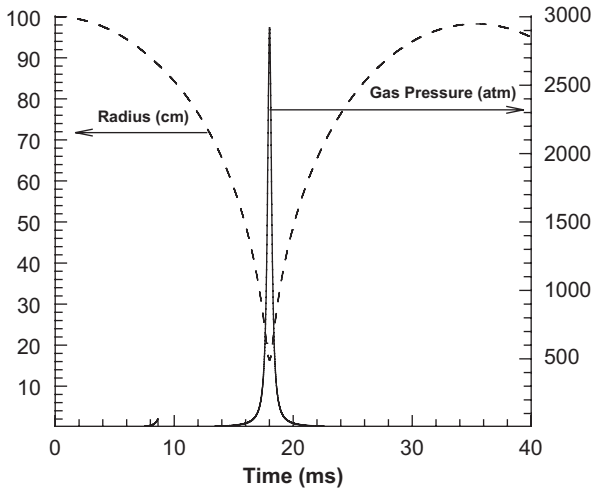

Fig. 17. Spherical volume radius and gas pressure under conditions given in Table 3, when the inner shell (plastic or elastic) fails.

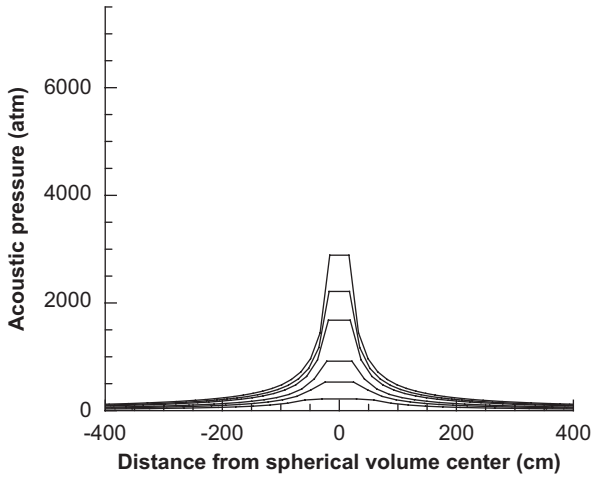

Fig. 18. Acoustic pressure in liquid surrounding spherical volume under conditions given in Table 3, when the inner shell (plastic or elastic) fails. In order of increasing magnitude, the data are presented at 17.36, 17.60, 17.72, 17.84, 17.90, and 18.02 ms (the time of peak magnitude of the acoustic field).

3.5. Failure of deformable shells

The analysis of the plastic and elastic shells was now modified so that they could both fail. The failure stress was the value given in Table 2. Failure of the elastic shell occurred at 8.63 ms at a pressure of 61.7 atm. Failure of the elastic sphere occurred at 8.50 ms at a pressure of 60.4 atm. At this point, the shell was assumed to have shattered and results are virtually the same for both the elastic and plastic shells.

Fig. 17 is a plot of the gaseous volume radius and pressure for the case where the shells failed. The maximum pressure in Fig. 17 is approximately an order of magnitude higher than shown in Figs. 11 and 15 for the plastic and elastic shells. The work that was done to compress the shells plastically or elastically is now available for compression of the gas

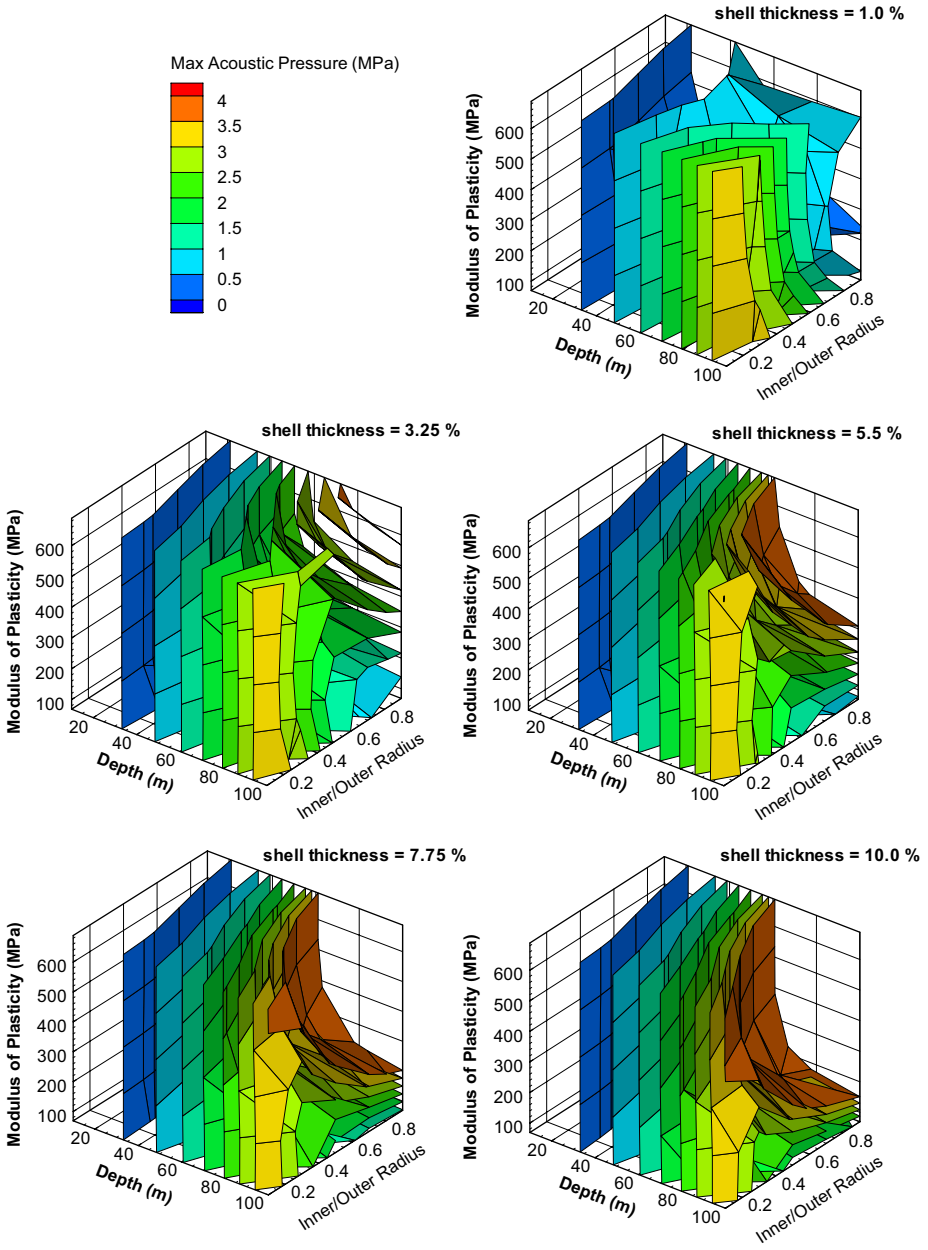

Fig. 19. Contour plots of maximum acoustic pressure at two times the initial outer volume diameter with plastic inner sphere with an initial outer shell radius of 10 cm.

volume, and the pressure in the gas is correspondingly higher. It is also noted that the volume's period oscillation has increased relative to the cases of shell deformation without failure.

Fig. 18 shows the acoustic pressure in the surrounding liquid when the shells are allowed to fail. Although the peak acoustic pressure is increased over that of Figs. 13(b) and 16, it is still significantly reduced over that shown in Fig. 13(a) for the infinitely strong shell case.

4. Parametric study

4.1. Non-destructible plastic inner shell

A parametric study was made of implodable volumes with a plastic inner structure over a range of conditions. Studies showed that the structures were relatively insensitive to the values of material viscosity and density chosen, so these

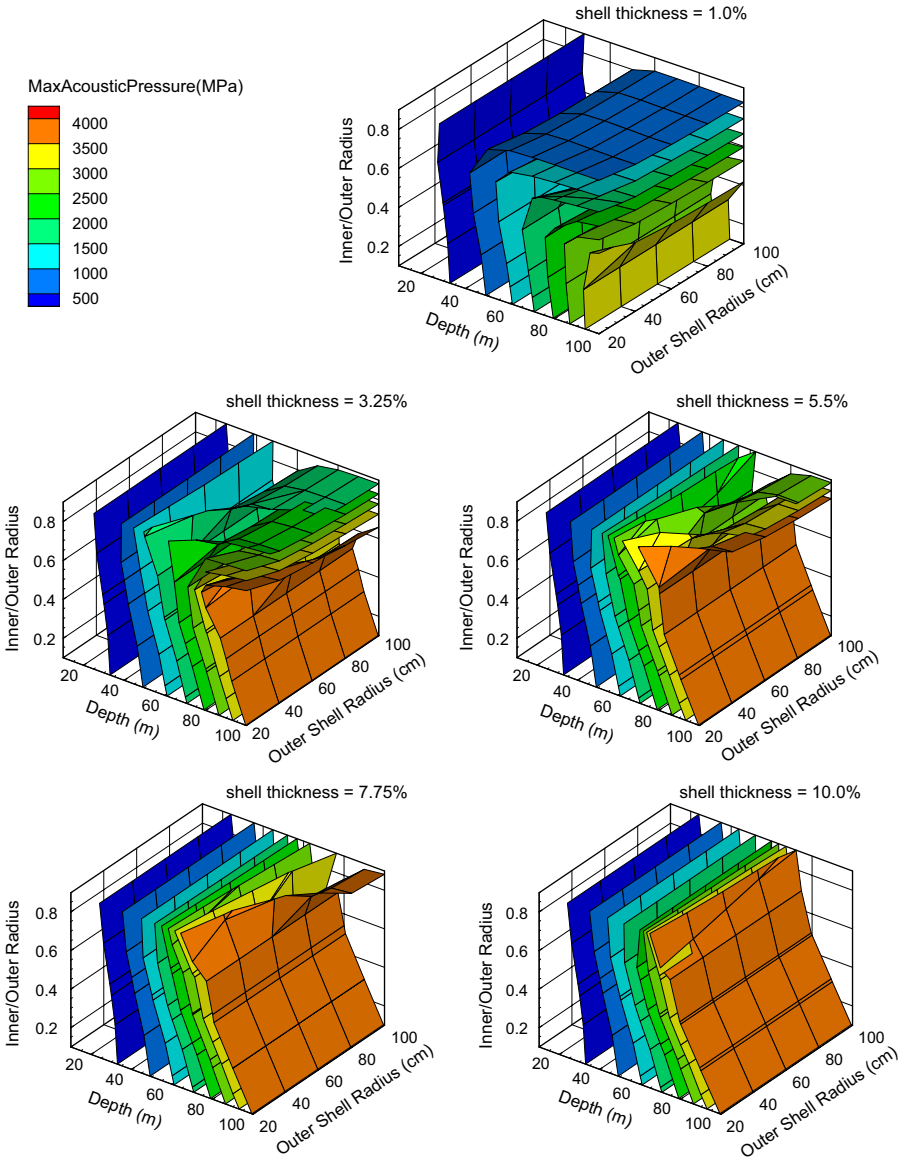

Fig. 20. Contour plots of maximum acoustic pressure at two times the initial outer volume diameter with an elastic inner sphere with a modulus of elasticity of 68 900 MPa.

values were assigned values of 7850 kg/m^3 and 4000 N s/m^2. Parameters which were then varied were the outer (pre-rupture) shell radius, the volume depth below the surface, the ratio of the inner-to-outer radius, and the inner shell thickness. The acoustic pressure was calculated at a distance of two times the outer shell radius. Fig. 19 is a set of contour plots for the maximum acoustic pressure at two initial gas volume radii with an initial outer shell radius of 10 cm. Axes plotted are the depth below the surface, the ratio of the initial inner plastic shell radius to the initial outer gas shell radius, and the material modulus of plasticity. The inner shell thicknesses are reported in percents of the initial plastic shell radius. The maximum acoustic pressure increases with the ratio of the radius of the inner shell to the initial radius of the outer volume. This is consistent with the finding discussed in the previous section, that the effect of the inner structure becomes more pronounced as its radius approaches that of the outer radius. The effect of the modulus of plasticity also only becomes apparent at high ratios of the inner to outer volume, where the effect of the inner structure

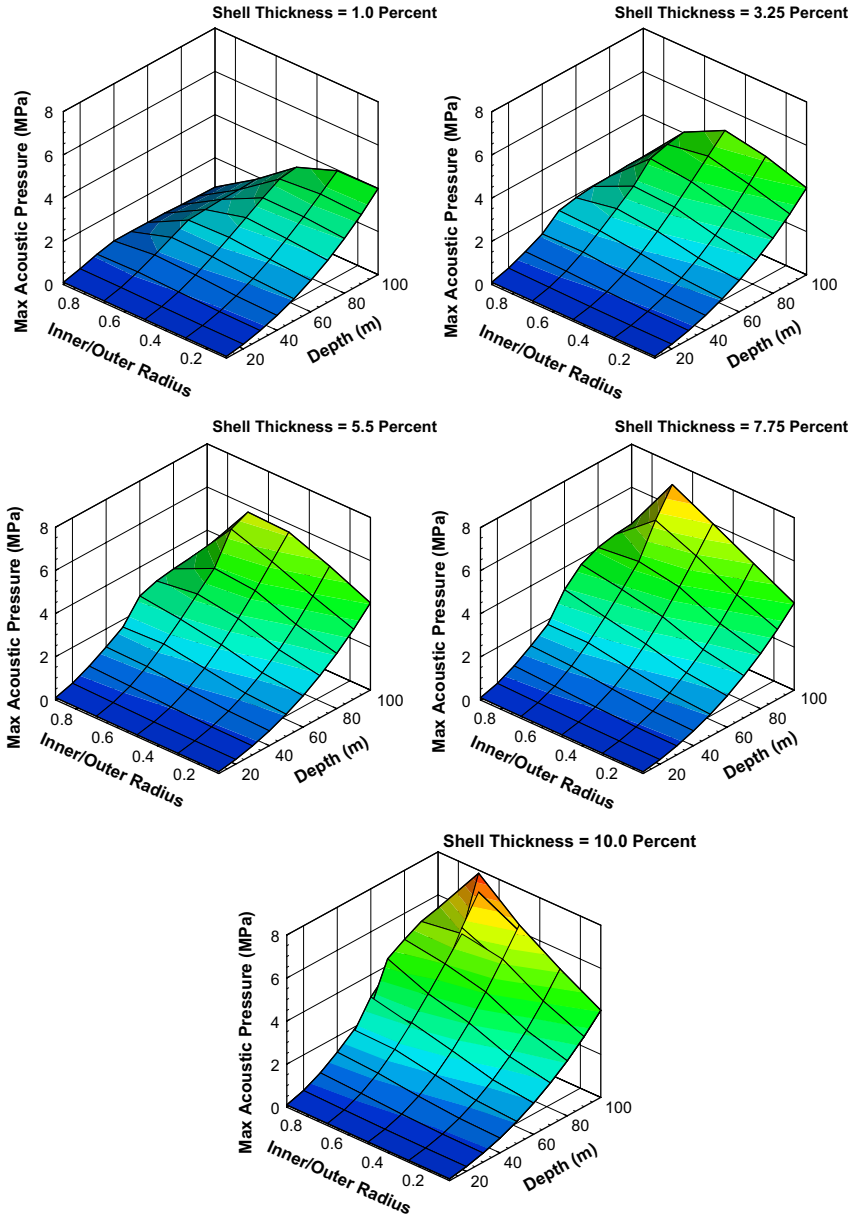

Fig. 21. Maximum acoustic pressure at two times the initial outer shell radius plotted against depth and the inner-to-outer radius ratio. The initial outer shell radius is 60 cm and the elastic modulus is 68 900 MPa.

is pronounced. The maximum acoustic pressure increases with depth because at greater depths the gaseous volume is compressed to a greater degree. Thicker inner shells increased the maximum acoustic pressure by making the inner structure stronger. The initial outer radius was increased up to 100 cm, but its effect on the final results was small.

4.2. Non-destructible elastic inner shell

A parametric study was made of implodable volumes with an elastic inner structure over a range of conditions. Parameters which were varied were the outer (pre-rupture) shell radius, the depth below the surface, the ratio of the inner-to-outer radius, and the inner shell thickness. The acoustic pressure was again calculated at a distance of two times the initial outer shell radius. Fig. 20 is a set of contour plots for the maximum acoustic pressure at this distance when the inner shell has an elastic modulus of 68 900 MPa. The axes in this figure have been changed to the initial outer shell radius, depth and ratio of inner to outer radius. Similar trends were shown in the parametric results when using an elastic modulus up to three times larger than used to generate Fig. 20. The coupling between the results and the value chosen for the outer shell's initial radius was found to be stronger than in the case of the plastic shell.

To better isolate the effects at play causing this coupling, the maximum acoustic pressure is plotted versus depth and the ratio of inner-to-outer radius in Fig. 21. These data are plotted for an outer shell radius of 60 cm and an elastic modulus of 68 900 MPa. The coloring in this figure is included to aid the eye in viewing the results. It can be seen that the maximum acoustic pressure peaks at different depths at different values for the inner-to-outer radius ratio. Below this ratio, the pressure build-up in the implosion event is less severe so the maximum acoustic pressure decreases. Above this peak ratio, the reduction in gas volume becomes large enough that the peak acoustic pressure again decreases.

4.3. Destructible inner shells

Parametric studies were conducted with elastic and plastic inner shells that were allowed to fail. Trends were found to be very similar whether elastic or plastic inner shells were used. Therefore, the results of the plastic inner shell parametric study will be presented as representative of both cases. For this study, the material viscosity was 4000 ($N\,s/m^2$), the material density was 7850 kg/m^3, the inner shell thickness was 10% and the plastic modulus was 345 MPa. Results showed relative insensitivity to the outer shell radius, and pronounced "saddle points" in the peak acoustic pressure at different depths and failure stresses. To investigate these "saddle points" further, data for the outer shell radius of 60 cm were examined in isolation. Fig. 22 shows a three-dimensional contour plot resulting from this analysis. As before, the contours are for the maximum acoustic pressure encountered at two initial outer volume radii. In this figure, the maximum acoustic pressure appears to follow different "orbits" around points in depth-compressive failure stress-inner/outer radius space.

The nature of these "orbits" was examined by plotting the maximum acoustic pressure against compressive failure stress and depth, as shown in Fig. 23. The coloring in this figure is included to aid the eye in viewing the results. The "saddle

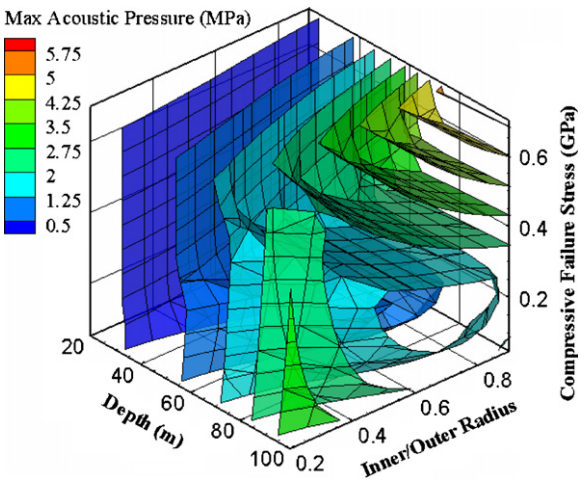

Fig. 22. Contour plots of maximum acoustic pressure at two times the initial outer volume diameter with a plastic inner sphere with a modulus of plasticity of 345 MPa and an initial outer radius of 60 cm.

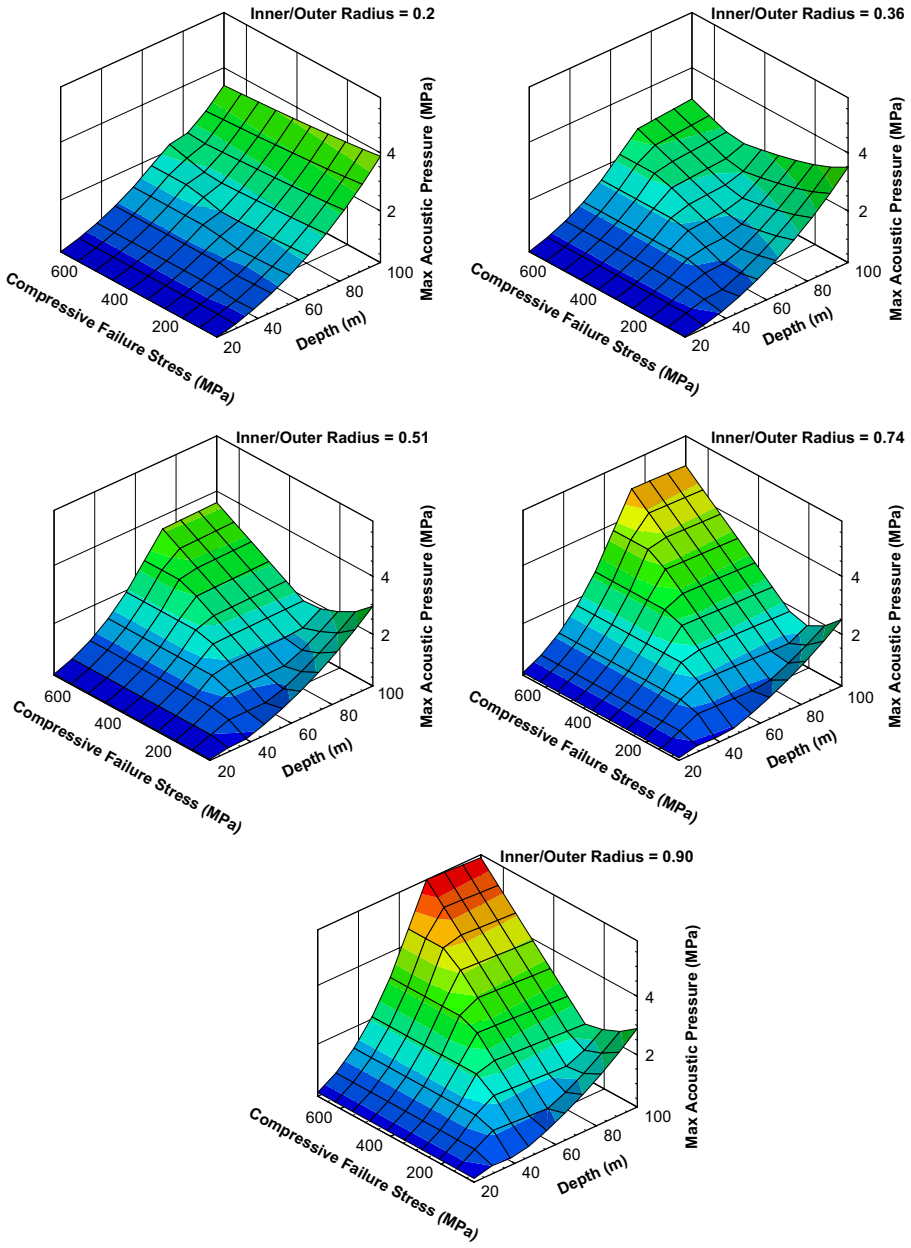

Fig. 23. Plots of maximum acoustic pressure at two times the initial outer volume diameter versus compressive failure stress and depth at the same conditions as in Fig. 22.

points" in Fig. 23 can be explained in terms of work done on the inner shell. At a given depth, there is a failure stress at which the minimum acoustic energy is found. At failure stresses lower than this value, the acoustic energy rises because progressively less energy is absorbed by the shell as it fails. As the failure stress is increased above this "saddle point" value, the growth in pressure inside the gaseous volume before failure starts to increase the maximum acoustic energy.

5. Conclusions

The above analyses indicate that an implodable volume interacting with the surrounding liquid can cause significant pressure pulses in the liquid medium. This is an important consideration for assessing the effect of the rupture of an

underwater container on nearby or enclosing structures. Large pressure excursions generated by the initial rupture have the potential to create damaging acoustic waves in the water. The analysis has also shown that the existence of any interior structure inside the ruptured container, and its physical properties, can strongly reduce the strength of acoustic waves in the surrounding liquid. The effect of an inner structure on the acoustic field in the liquid becomes most significant when initial volumes of the inner and outer structure are of comparable sizes. While we do not pretend that the above analysis has been complete or exhaustive, we believe that it points out a need for—and suggests possible directions for—more detailed and thorough studies that can quantify the level of conservatism in current undersea vehicle safety guidelines.

Future analysis should focus on the nature of the gas pressure field in the presence of an interior structure, the shape of the inner structure, and nonuniform structural failure. As mentioned above, the failure of the inner structure has the potential to initiate an imploding shock wave in the gas volume, and analysis developed for this scenario could prove illuminating. Incorporating a work effect due to any deformation of the inner volume on the pressure in the surrounding outer gas would be a significant contribution as well.

Acknowledgment

The authors gratefully acknowledge the support of the Office of Naval Research under N00014-05-6-106 and administrator Dr Kam Ng.

References

Arons, A.B., Slifko, J.P., Carter, A., 1948. Secondary pressure pulses due to gas globe oscillation in underwater explosions. I. Experimental data. The Journal of the Acoustic Society of America 20 (3), 271–276.

Ghiotto, A., Penrose, J.D., 2000. Investigating the acoustic properties of the underwater implosions of light globes and evacuated spheres. In: Australian Acoustical Society Conference, Joondalup, Australia, 15–17 November, pp. 1–8.

Goodwin, R., Chapyak, E., Noack, J., Vogel, A., 1999. Aspherical bubble dynamics and oscillation times. In: SPIE Conference on Laser–Tissue Interaction X:Photochemcial, Photothermal and Photomechanical, San Jose, CA, January 1999.

Iakovlev, S., 2004. Influence of a rigid coaxial core on the stress–strain state of a submerged fluid-filled circular cylindrical shell subjected to a shock wave. Journal of Fluids and Structures 19 (7), 957–984.

Iakovlev, S., 2006. Submerged fluid-filled cylindrical shell subjected to a shock wave: fluid–structure interaction effects. Journal of Fluids and Structures 23 (1), 117–142.

Joint Fleet Maintenance Manual, vol. 5, Part III. Department of the Navy, SUBMEPP, P.O. Box 2500, Portsmouth Naval Shipyard, New Hampshire, 11 April 2006, p. V-III-FWD-B-3.

Kalumuck, K.M., Duraiswami, R., Chahine, G.L., 1995. Bubble dynamics fluid–structure interaction simulation by coupling fluid BEM and structural FEM codes. Journal of Fluids and Structures 9 (8), 861–883.

Klaseboer, E., Khoo, B.C., Hung, K.C., 2005. Dynamics of an oscillating bubble near a floating structure. Journal of Fluids and Structures 21 (4), 395–412.

Lamb, Sir H., 1932. Hydrodynamics, sixth ed. Dover Publications, New York, pp. 122–123.

The Navy Unmanned Undersea Vehicle (UUV) Master Plan. Department of Navy (approved for public release; distribution unlimited), 9 November 2004, p. 93.

Rayleigh, L., 1917. On the pressure developed in a liquid during the collapse of a spherical cavity. Philosophical Magazine 34, 94–98.

Tan, D., Sun, C., Yanping, W., 2003. Acceleration and viscoplastic deformation of spherical and cylindrical casings under explosive loading. Propellants, Explosives, Pyrotechnics 20 (1), 43–47.

Vokurka, K., 1985. On Rayleigh's model of a freely oscillating bubble. I. Basic relations. Czechoslovak Journal of Physics, Section B 35, 28–40.

Zong, Z., 2004. A hydroplastic analysis of a free–free beam floating on water subjected to an underwater bubble. Journal of Fluids and Structures 20 (3), 372–395.